Cell Metabolism

Resource

Isotope tracing in adult zebrafish reveals alanine cycling between melanoma and liver

Graphical abstract

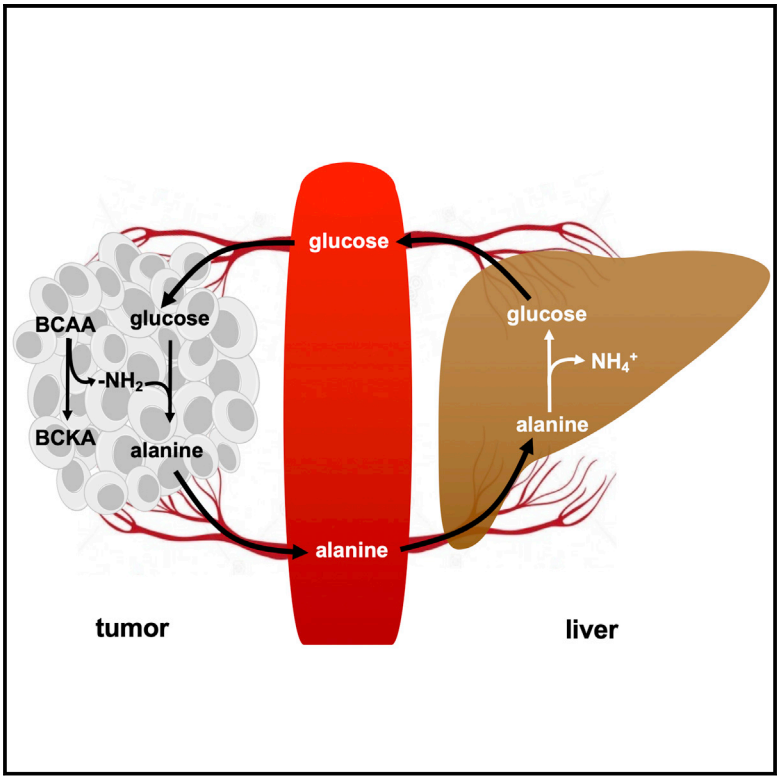

Authors

Fuad J. Naser, Madelyn M. Jackstadt, Ronald Fowle-Grider, ..., Leah P. Shriver, Stephen L. Johnson, Gary J. Patti

Correspondence

gjpattij@wustl.edu

In brief

Using a workflow they established for isotope tracing in adult zebrafish, Naser et al. provide evidence that non-malignant tissues alter their metabolism to support tumor growth. They demonstrate that glucose-derived alanine is excreted from melanoma and transferred to the liver for gluconeogenesis. Pharmacologically impairing this metabolite exchange decreases tumor burden.

Highlights

- Adult zebrafish are well suited for steady-state labeling and metabolomics
- Branched-chain amino acid catabolism by melanoma contributes to alanine excretion
- Glucose-derived alanine excreted from the tumor is used for hepatic gluconeogenesis
- Pharmacological inhibition of the tumor-liver alanine cycle reduces tumor burden

Naser et al., 2021, Cell Metabolism *33*, 1–12
July 6, 2021
https://doi.org/10.1016/j.cmet.2021.04.014

CellPress

Please cite this article in press as: Naser et al., Isotope tracing in adult zebrafish reveals alanine cycling between melanoma and liver, Cell Metabolism (2021), https://doi.org/10.1016/j.cmet.2021.04.014

Cell Metabolism

CellPress

Resource

Isotope tracing in adult zebrafish reveals alanine cycling between melanoma and liver

Fuad J. Naser,[1,2,9] Madelyn M. Jackstadt,[1,2,9] Ronald Fowle-Grider,[1,2] Jonathan L. Spalding,[1,2,3] Kevin Cho,[1,2] Ethan Stancliffe,[1,2] Steven R. Doonan,[1,2] Eva T. Kramer,[2,4,5] Lijun Yao,[3,6,7] Bradley Krasnick,[7,8] Li Ding,[2,3,6,7] Ryan C. Fields,[7,8] Charles K. Kaufman,[2,4,5,7] Leah P. Shriver,[1,2] Stephen L. Johnson,[3,5] and Gary J. Patti[1,2,7,10,*]

[1]Department of Chemistry, Washington University in St. Louis, St. Louis, MO, USA
[2]Department of Medicine, Washington University in St. Louis, St. Louis, MO, USA
[3]Department of Genetics, Washington University in St. Louis, St. Louis, MO, USA
[4]Division of Medical Oncology, Washington University in St. Louis, St. Louis, MO, USA
[5]Department of Developmental Biology, Washington University in St. Louis, St. Louis, MO, USA
[6]McDonnell Genome Institute, Washington University in St. Louis, St. Louis, MO, USA
[7]Siteman Cancer Center, Washington University in St. Louis, St. Louis, MO, USA
[8]Department of Surgery, Washington University in St. Louis, St. Louis, MO, USA
[9]These authors contributed equally
[10]Lead contact
*Correspondence: gjpattij@wustl.edu
https://doi.org/10.1016/j.cmet.2021.04.014

SUMMARY

The cell-intrinsic nature of tumor metabolism has become increasingly well characterized. The impact that tumors have on systemic metabolism, however, has received less attention. Here, we used adult zebrafish harboring *BRAF*^{V600E}-driven melanoma to study the effect of cancer on distant tissues. By applying metabolomics and isotope tracing, we found that melanoma consume ~15 times more glucose than other tissues measured. Despite this burden, circulating glucose levels were maintained in disease animals by a tumor-liver alanine cycle. Excretion of glucose-derived alanine from tumors provided a source of carbon for hepatic gluconeogenesis and allowed tumors to remove excess nitrogen from branched-chain amino acid catabolism, which we found to be activated in zebrafish and human melanoma. Pharmacological inhibition of the tumor-liver alanine cycle in zebrafish reduced tumor burden. Our findings underscore the significance of metabolic crosstalk between tumors and distant tissues and establish the adult zebrafish as an attractive model to study such processes.

INTRODUCTION

Many studies have examined the autonomous effects of transformation on cellular metabolism (Vander Heiden et al., 2009). It is now well established that tumors adapt their metabolic activities to support the demands of rapid proliferation (DeBerardinis and Chandel, 2016; Vander Heiden and DeBerardinis, 2017). The impact that a tumor has on whole-body metabolism, however, remains poorly understood.

Of particular relevance is the avidity with which cancer cells consume nutrients ranging from glucose and lactate to lipids and amino acids (Chen et al., 2016; DeBerardinis et al., 2007; Gao et al., 2019; Hui et al., 2017; Jain et al., 2012; Kamphorst et al., 2013; Krall et al., 2016; Yao et al., 2016). Other tissues in a healthy organism rely on a stable supply of these same substrates to maintain their normal functions. Thus, the question arises of how the nutritional burdens of a tumor impact the metabolic physiology of a host. Although otherwise healthy tissues may compete with cancer cells for some of the same resources, it is also possible that the metabolic roles of organs within the host get redefined to complement the needs of the tumor. The objective of this work is to investigate tumor-induced changes in whole-body metabolism at the molecular level, which may improve our understanding of systemic pathologies, such as cachexia, that are associated with cancer.

To evaluate the relationship between tumor and host metabolism, we applied a *BRAF*^{V600E} mutant; *p53*-deficient genetic model of melanoma in zebrafish (Patton et al., 2005). Having all of the organs needed for metabolic control in humans, the adult zebrafish is well suited as an *in vivo* system to study metabolic physiology (White et al., 2013; Zang et al., 2018). A major advantage of zebrafish over mice and other mammalian systems is the technical convenience of performing isotope-tracer studies. Similar to cell culture, isotope tracers can simply be added to the tank water of animals where they are then taken up through the gills, skin, and mouth of zebrafish (Dang et al., 2016a; Truong et al., 2014). In contrast to mammalian systems, isotope tracers can therefore be continuously delivered to animals over an extended period of time without surgical pumps, injections, anesthesia, or the need to constrain animal movement (Davidson et al., 2016; Faubert

Please cite this article in press as: Naser et al., Isotope tracing in adult zebrafish reveals alanine cycling between melanoma and liver, Cell Metabolism (2021), https://doi.org/10.1016/j.cmet.2021.04.014

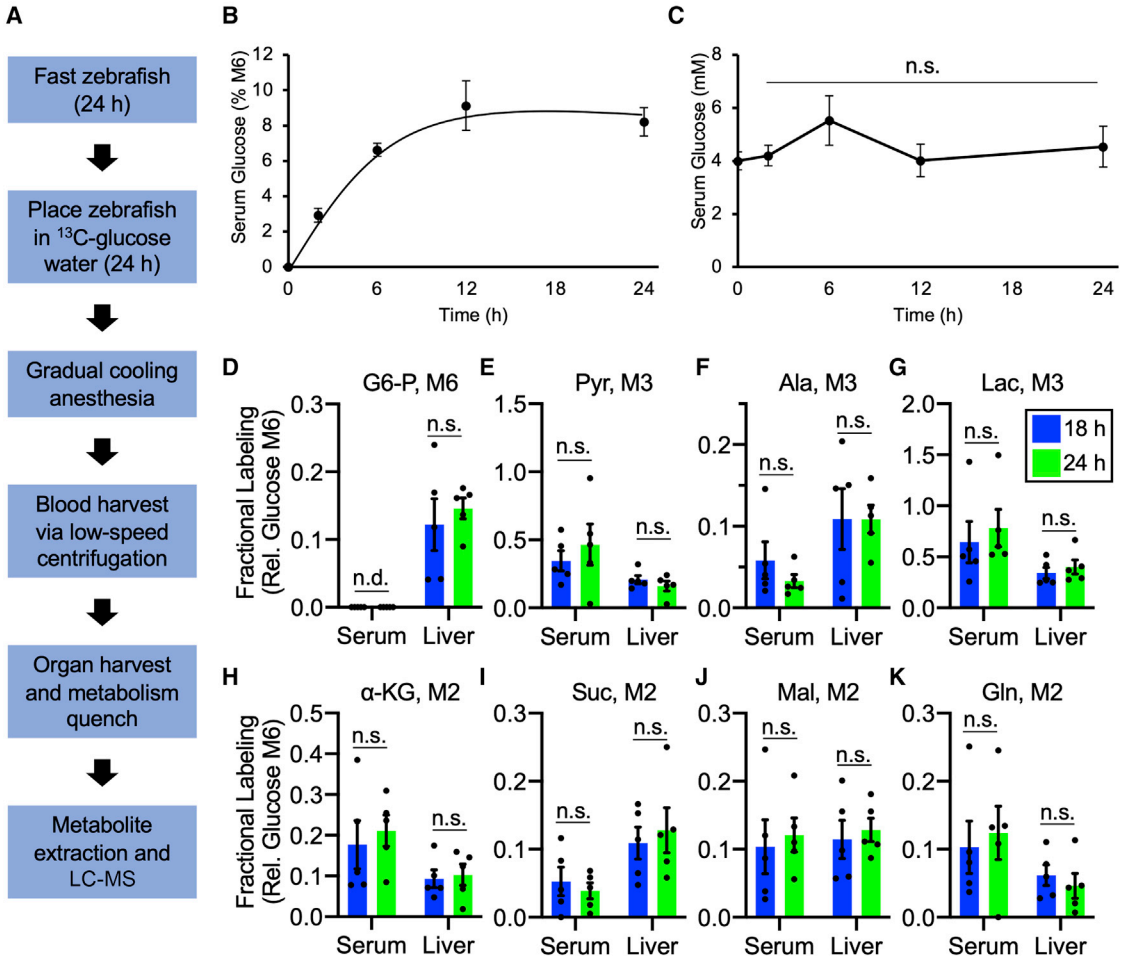

Figure 1. Adding isotope tracers to adult zebrafish water achieves isotopic steady-state labeling

(A) Schematic of the steady-state labeling workflow for LC-MS-based metabolomics.

(B) Kinetics to achieve steady-state labeling for serum glucose from WT zebrafish in tank water containing 10 mM [U-^{13}C] glucose. Values are mean ± SEM; n = 3–4 zebrafish per time point.

(C) Serum glucose levels in WT zebrafish over the course of 10 mM [U-^{13}C] glucose labeling. Values are mean ± SEM; n = 3–4 zebrafish per time point.

(D–G) Fractional labeling, relative to serum M6 glucose, of the glycolytic intermediates glucose 6-phosphate (D), pyruvate (E), alanine (F), and lactate (G) in WT serum and liver between 18 and 24 h. Data are mean ± SEM; n = 5 zebrafish per time point.

(H–K) Fractional labeling, relative to serum M6 glucose, of the metabolites α-ketoglutarate (H), succinate (I), malate (J), and glutamine (K) in WT serum and liver between 18 and 24 h. Data are mean ± SEM; n = 5 zebrafish per time point.

n.d., not detected; n.s., not statistically significant according to a two-tailed paired t test; G6-P, glucose 6-phosphate; Pyr, pyruvate; Ala, alanine; Lac, lactate; α-KG, α-ketoglutarate; Suc, succinate; Mal, malate; Gln, glutamine. Full labeling data are available in Data S1.

et al., 2017; Hui et al., 2017; Jang et al., 2019). This minimizes animal stress and hence permits a more representative measurement of metabolism with significantly reduced technical difficulty for the researcher (Fernández-García et al., 2020).

RESULTS AND DISCUSSION

Isotope tracing in single adult zebrafish

Given that isotope-tracer studies have not yet been performed in adult zebrafish, we first established a workflow for the experiments (Figure 1A). The relatively small size of zebrafish complicates metabolomics analysis of serum and tissues from individual animals. To obtain sufficient serum for liquid chromatography-mass spectrometry (LC-MS) analysis from a single fish, we adapted a method that has been applied in proteomics (Babaei et al., 2013). In brief, following caudal fin amputation, animals were subjected to low-speed centrifugation to collect blood (Figure S1A). We also applied nonchemical anesthesia during the process, which we found led to more reliable measurements of metabolism compared with the commonly used tricaine methods (Figure S1B) (Eames et al., 2010).

Once we had an experimental workflow in place to make metabolomics measurements from individual zebrafish, we next sought to optimize conditions for achieving isotopic steady state. Although isotopic steady state is not required to perform isotope tracing, it can simplify interpretation of the data (Buescher et al., 2015). Wild-type (WT) fish were fasted and then transferred to tank water containing [U-^{13}C] glucose at a

Please cite this article in press as: Naser et al., Isotope tracing in adult zebrafish reveals alanine cycling between melanoma and liver, Cell Metabolism (2021), https://doi.org/10.1016/j.cmet.2021.04.014

concentration of 5–20 mM. Within 24 h, all of the concentrations tested led to isotopic steady state for circulating glucose (Figures 1B and S1C). We determined that the 10 mM condition was optimal because it maximized labeling of downstream metabolites while not causing any significant perturbations in circulating glucose levels (Figures 1C and S1D). Moreover, after 24 h, no significant alterations in metabolism were detected in animals transferred to tank water containing 10 mM glucose compared with control animals maintained under standard conditions (Figures S1E–S1K). To ensure that isotopic steady state was achieved systemically after placing zebrafish in 10 mM [U-^{13}C] glucose water for 24 h, we also compared the fractional labeling of key central carbon metabolites in serum and liver with LC-MS. Fractional labeling is defined as the fraction of a given isotopologue for a metabolite normalized to the fraction of [U-^{13}C] tracer in the circulation. Labeling of glycolytic metabolites, TCA cycle metabolites, and related amino acids were at isotopic steady state across the whole organism (Figures 1D–1K).

Normalized labeling, defined as the percentage of ^{13}C atoms in a metabolite normalized to the percentage of ^{13}C atoms in a circulating tracer, has been used to assess the direct and indirect contributions of a tracer at isotopic steady state to a downstream metabolite *in vivo* (Hui et al., 2017). On the basis of normalized labeling, we found that the glucose contribution to circulating lactate and glutamine in zebrafish (~70% and ~10%, respectively) was comparable to mice (~65% and ~10%, respectively) (Figure S1L) (Hui et al., 2017). Additionally, the contribution of glucose to the TCA cycle in most zebrafish tissues (e.g., ~15% in liver, ~12% in muscle, and ~7% in intestine) was similar to the corresponding mouse tissues (e.g., ~15% in liver, ~20% in muscle, and ~10% in intestine) (Figure S1L) (Hui et al., 2017). These findings indicate that the isotope-tracing results from glucose are largely conserved between WT zebrafish and mice.

Application to a zebrafish melanoma model

Having established our experimental workflow, we sought to explore alterations in whole-body metabolism due to cancer by using a zebrafish model of melanoma. Transgenic expression of the human oncogenic *BRAF^{V600E}* mutation under the control of the melanocyte *mitfa* promoter in a *p53*-deficient background leads to spontaneous melanoma development (Patton et al., 2005). Previous work has demonstrated that, *in vitro*, *BRAF^{V600E}*-driven melanoma cells are glutamine addicted, consuming up to 7-fold more glutamine than normal melanocytes (Scott et al., 2011). In cell culture studies, *BRAF^{V600E}*-driven melanoma cells rely on glutamine as a precursor for TCA cycle intermediates and related metabolites such as proline and asparagine (Ratnikov et al., 2015, 2017). Thus, we hypothesized that a demand to sustain the TCA cycle with circulating glutamine carbon may represent a metabolic burden of melanoma on the organism. To test this idea, we placed BRAF/p53 (*BRAF^{V600E}* mutant; *p53* deficient) zebrafish in 5 mM [U-^{13}C] glutamine for 24 h to achieve isotopic steady state. We determined that these conditions were optimal for achieving steady-state labeling of serum glutamine without perturbation of circulating glutamine levels (Figures S2A and S2B). Surprisingly, in contrast to previous *in vitro* studies, our *in vivo* data showed that glutamine contributed only minimally to the TCA cycle in melanoma (Figures 2A and S2C). We point out that the fraction of labeled glutamine in melanoma matched that of the circulation, which indicates that low glutamine uptake was not the cause of the small contribution of glutamine to the TCA cycle in melanoma (Figure 2B). Indeed, the contribution of glutamine to the TCA cycle in melanoma was comparable to fin tissue, which contains a high concentration of normal melanocytes (Figure S2C). Liver and intestine, on the other hand, showed more extensive incorporation of glutamine carbon (Figure S2C). Our observations are consistent with other studies demonstrating that, for some cancers, glutamine utilization is decreased *in vivo* compared with that *in vitro* (Davidson et al., 2016; Hensley et al., 2016). Given these results, it seemed unlikely that glutamine utilization by melanoma significantly impacted whole-body metabolism.

In addition to being glutamine addicted, *BRAF^{V600E}*-expressing melanoma cells are also known to increase their consumption of glucose relative to normal melanocytes *in vitro* (Scott et al., 2011). We therefore examined utilization of glucose *in vivo* by placing BRAF/p53 zebrafish in 10 mM [U-^{13}C] glucose for 24 h to achieve isotopic steady state (Figure 2C). We found that glucose contributed significantly more carbon than glutamine to glycolysis, the TCA cycle, and related amino acids (Figures 2A, 2C, and 2D). Additionally, all tissues with the exception of brain showed lower levels of labeling in glycolytic intermediates relative to tumor (Figure S2D). To assess the flux of glycolysis in melanoma directly, we administered 0.5 mg of [U-^{13}C] glucose per gram of zebrafish via intraperitoneal injection and labeling in lactate was measured from various tissues as a function of time (Figure 2E). The results demonstrate that the flux of glucose to lactate in melanoma is significantly higher than in other tissues, such as liver and muscle. From these data, we predicted that tumors were consuming more glucose than other tissues. To assess glucose uptake, we placed BRAF/p53 fish in 1 mM 2-deoxyglucose (2-DG). Similar to glucose, 2-DG is taken up by glucose transporters and metabolized to 2-deoxyglucose 6-phosphate (2-DG6-P). Notably, 2-DG6-P cannot be further metabolized in cells, and it accumulates as a function of uptake rate. We quantified the relative concentrations of 2-DG6-P in tissues and determined that tumors consume 16- and 14-fold more glucose than the liver and muscle, respectively (Figure 2F). In spite of this pathological demand for glucose introduced by the tumor, however, we found that circulating glucose levels were not different in BRAF/p53 fish as compared with WT (Figure 2G). Additionally, glycolytic flux was not altered in muscle, showing that glucose was still being used as a fuel in non-malignant tissues (Figure S2E).

Impact of melanoma on whole-body metabolism

Our findings demonstrate that BRAF/p53 animals are able to maintain glucose homeostasis, even in the face of the metabolic burden imposed by the tumor. The data suggest that, while some tissues may compete with melanoma for glucose, other tissues are likely to reprogram their metabolism to complement the tumor. To evaluate the impact of melanoma on whole-body metabolism, we used LC-MS-based metabolomics to profile tissues from BRAF/p53 zebrafish after administration of an isotopically labeled glucose tracer. WT and melanoma-bearing zebrafish were placed in 10 mM [U-^{13}C] glucose for 24 h to achieve isotopic steady state, and ^{13}C-enrichment and pool sizes of metabolites from WT were

Please cite this article in press as: Naser et al., Isotope tracing in adult zebrafish reveals alanine cycling between melanoma and liver, Cell Metabolism (2021), https://doi.org/10.1016/j.cmet.2021.04.014

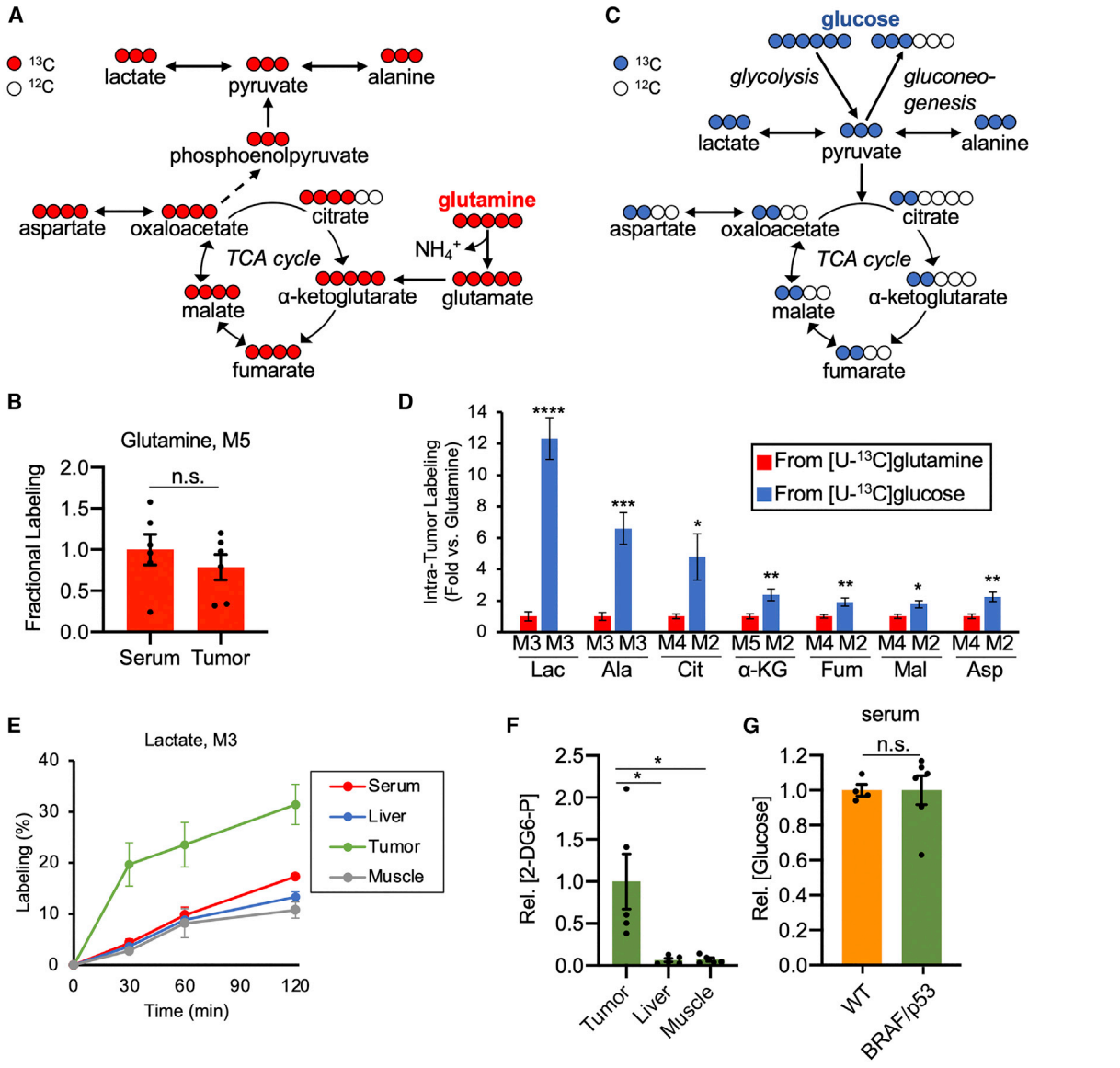

Figure 2. Glucose is a major carbon source for melanoma metabolism *in vivo*

(A) Schematic to illustrate the transformation of glutamine carbon to key intermediates in central carbon metabolism.

(B) Fractional labeling in tumor M5 glutamine, normalized to serum M5 glutamine, from a [U-^{13}C] glutamine tracer. Values are mean ± SEM; n = 6 zebrafish.

(C) Schematic to illustrate the transformation of glucose carbon to key intermediates in central carbon metabolism.

(D) Comparison of the ^{13}C-contribution from glucose and glutamine tracers to central carbon metabolites in melanoma. As expected, the isotopologues shown accounted for the majority of the labeling. Data shown here are presented as fold changes (i.e., the amount of labeling from [U-^{13}C] glucose relative to the amount of labeling from [U-^{13}C] glutamine, which is normalized to 1). Values are mean ± SEM; n = 6–10 zebrafish per condition.

(E) Absolute enrichment of lactate (M3 isotopologue) over time in tissues from BRAF/p53 zebrafish following an intraperitoneal injection of [U-^{13}C] glucose. Data are mean ± SEM; n = 3–4 zebrafish per time point.

(F) Glucose uptake in tissues from BRAF/p53 zebrafish. Relative concentration of 2-deoxyglucose 6-phosphate (2-DG6-P) for tissues within a fish are normalized to the 2-DG6-P pool in its tumor. Values are mean ± SEM; n = 5–6 zebrafish per condition.

(G) Relative pool size of circulating glucose in WT and BRAF/p53 fish, normalized to the WT group. Values are mean ± SEM; n = 4–6 zebrafish per condition.

Statistically significant differences were assessed by a two-tailed paired t test and annotated as follows: *p < 0.05, **p < 0.01, ***p < 0.001, ****p < 0.0001, or n.s. = not significant. Lac, lactate; Ala, alanine; Cit, citrate; α-KG, α-ketoglutarate; Fum, fumarate; Mal, malate; Asp, aspartate. Full labeling data are provided in Data S2.

compared with BRAF/p53 animals (Figures 3A and 3B). Seven different sample types were individually examined: liver, intestine, fin, muscle, brain, serum, and eye. Interestingly, we observed metabolic dysregulation across most tissues in BRAF/p53 fish, indicating that melanoma broadly impacts organismal glucose metabolism. Elucidating the mechanisms underlying all of these metabolic changes is beyond the scope of the current work, but we include the data here as a resource to provide an integrative picture of alterations in whole-body metabolism that occur due to the presence of a tumor (Figures 3A and 3B; Data S3).

Please cite this article in press as: Naser et al., Isotope tracing in adult zebrafish reveals alanine cycling between melanoma and liver, Cell Metabolism (2021), https://doi.org/10.1016/j.cmet.2021.04.014

Given the magnitude of changes observed in the liver of tumor-bearing animals and the role of this organ in maintaining glucose homeostasis, we focused our attention here (Figures 3A and 3B). We reasoned that the livers of BRAF/p53 fish might be increasing *de novo* glucose production as a compensatory measure in response to melanoma to maintain glucose homeostasis (Figure 2G). Hepatic glucose production occurs primarily through two mechanisms: hydrolysis of glucose from glycogen (i.e., glycogenolysis) and production of new glucose molecules from non-carbohydrate precursors via gluconeogenesis. Glycogen accounts for as much as 15% of the total liver mass, and its degradation is the first mechanism activated to maintain systemic glucose levels (Bonjorn et al., 2002). Consistent with increased glycogenolysis, we found that the livers of BRAF/p53 fish had a significant reduction in glycogen content relative to the livers from WT fish as confirmed by a quantitative assay, periodic acid-Schiff staining, and decreased liver mass (Figures 3C and S3A–S3C). Although the expression of genes involved in gluconeogenesis was unaltered in livers between WT and BRAF/p53 fish, data from [U-^{13}C] glucose tracing revealed increased substrate flux through gluconeogenesis in disease animals (Figures 3D and 3E). Specifically, we observed an increase in M3 glucose labeling in the serum and livers of BRAF/p53 fish, which is a signature of gluconeogenesis (Figure 3E). Additionally, increased M3 malate labeling in the livers of fish with melanoma further supported higher gluconeogenic flux via pyruvate carboxylase (Figures S3D and S3E) (Buescher et al., 2015).

Tumor-liver alanine cycle

We surmised that there were three candidates most likely to be used as gluconeogenic substrates by the liver of BRAF/p53 animals to support increased glucose production: lactate, alanine, and pyruvate. Lactate is the most abundant circulating three-carbon metabolite derived from glucose, is typically excreted at high concentrations by tumors, and is a well-established substrate for hepatic gluconeogenesis in healthy animals (Ross et al., 1967; Vander Heiden et al., 2009). M3 labeling of lactate, however, was not elevated in the circulation or liver of BRAF/p53 animals, despite it being readily produced by tumors (Figure 3F). Thus, it seemed unlikely that lactate was used as a substrate to support increased gluconeogenesis in fish with melanoma. In contrast, M3 labeling of alanine was significantly increased in both the circulation and the liver of disease animals (Figure 3G). Furthermore, M3 labeling of pyruvate was elevated in the livers, but not serum of BRAF/p53 fish (Figure 3H). These data are consistent with the liver taking up more alanine from the circulation and transforming it into pyruvate within the liver to use as a substrate for gluconeogenesis (Figures 2C, 3G, and 3H).

Conventionally, muscle is thought of as the major source of alanine production and participates in inter-organ alanine exchange with liver (Felig, 1973). Notably, in tumor-bearing animals, our data indicate a different paradigm of metabolite exchange where the main source of alanine for gluconeogenesis is melanoma rather than muscle. Two observations support this claim. First, M3 labeling of alanine was over 2-fold higher in tumor relative to muscle (Figure 3I). Second, the relative labeling of M3 alanine was not statistically different between melanoma and liver (Figure 3I). To confirm tissue uptake of alanine and the directionality of alanine transfer, we placed BRAF/p53 zebrafish in tank water containing 0.5 mM of the non-metabolizable alanine analog 2-aminoisobutyric acid (2-AIB). Measurement of 2-AIB levels in tissue provides a proxy for alanine uptake (Akedo and Christensen, 1962; Edmondson et al., 1979). We compared the concentrations of 2-AIB in liver, tumor, and muscle and found that relative alanine uptake in liver was ~3-fold higher than in melanoma. In contrast, the amount of alanine taken up by melanoma was similar to that of muscle (Figure 3J). Taken together, our data show that melanoma produce more alanine than muscle and take up less alanine than liver, thereby supporting that melanoma-derived alanine contributes to a non-conventional tumor-liver alanine cycle to replenish circulating glucose in animals with tumors.

The alanine cycle removes excess nitrogen from catabolism of branched-chain amino acids

In vertebrates, the liver plays a major role in maintaining systemic nitrogen homeostasis (Haüssinger, 1990). In contrast to urea excretion in mammals, however, the primary process by which zebrafish remove nitrogenous waste is ammonotelism, where liver-produced ammonia from amino acid catabolism is excreted directly through the gills (Braun et al., 2009; Randall and Wright, 1987). This waste-removal mechanism (and other processes like it) exemplify another advantage of using zebrafish in metabolism research: tank water can be sampled repeatedly and non-invasively to measure excretory molecules derived from metabolic processes. As such, we examined whether tumor-liver alanine cycling in BRAF/p53 fish was associated with aberrant ammonia excretion compared with WT fish. BRAF/p53 and WT fish were housed separately in fresh water, and ammonia levels were measured after 24 h. In agreement with pathological alanine cycling, animals with tumors excreted nearly twice as much ammonia as WT fish (Figure 4A).

We were next interested in determining the source of the nitrogen being excreted from tumors. We first considered the uptake of circulating protein through macropinocytosis, a process known to provide an important source of nutrients for pancreatic tumors (Davidson et al., 2017). We reasoned that oxidation of the carbon skeletons of protein-derived amino acids could lead to an excess of intracellular nitrogen that needed to be removed. To assess the potential contribution of protein uptake to nitrogen balance, we treated tumor-bearing animals with the macropinocytosis inhibitor 5-(N-ethyl-N-isopropyl)amiloride (EIPA) and then examined alanine cycling. Even at high concentrations, EIPA did not affect alanine labeling in the tumor or hepatic gluconeogenesis (as reflected by M3 labeling of glucose in the liver and serum). These data indicate that macropinocytosis does not provide a significant contribution to the nitrogen balance of tumors in our model (Figure 4B).

As an alternative source of nitrogen, we considered a second possibility that tumors might take up free amino acids directly from the circulation. We surmised that the most abundant amino acids in the serum of zebrafish would be likely to contribute the most nitrogen. With LC-MS-based metabolomics, we determined that the amino acids at the highest concentration in the serum of both WT and BRAF/p53 zebrafish are isoleucine, leucine, phenylalanine, glutamine, alanine, and valine (Figure S4A). Our previous data show that the contribution of

Please cite this article in press as: Naser et al., Isotope tracing in adult zebrafish reveals alanine cycling between melanoma and liver, Cell Metabolism (2021), https://doi.org/10.1016/j.cmet.2021.04.014

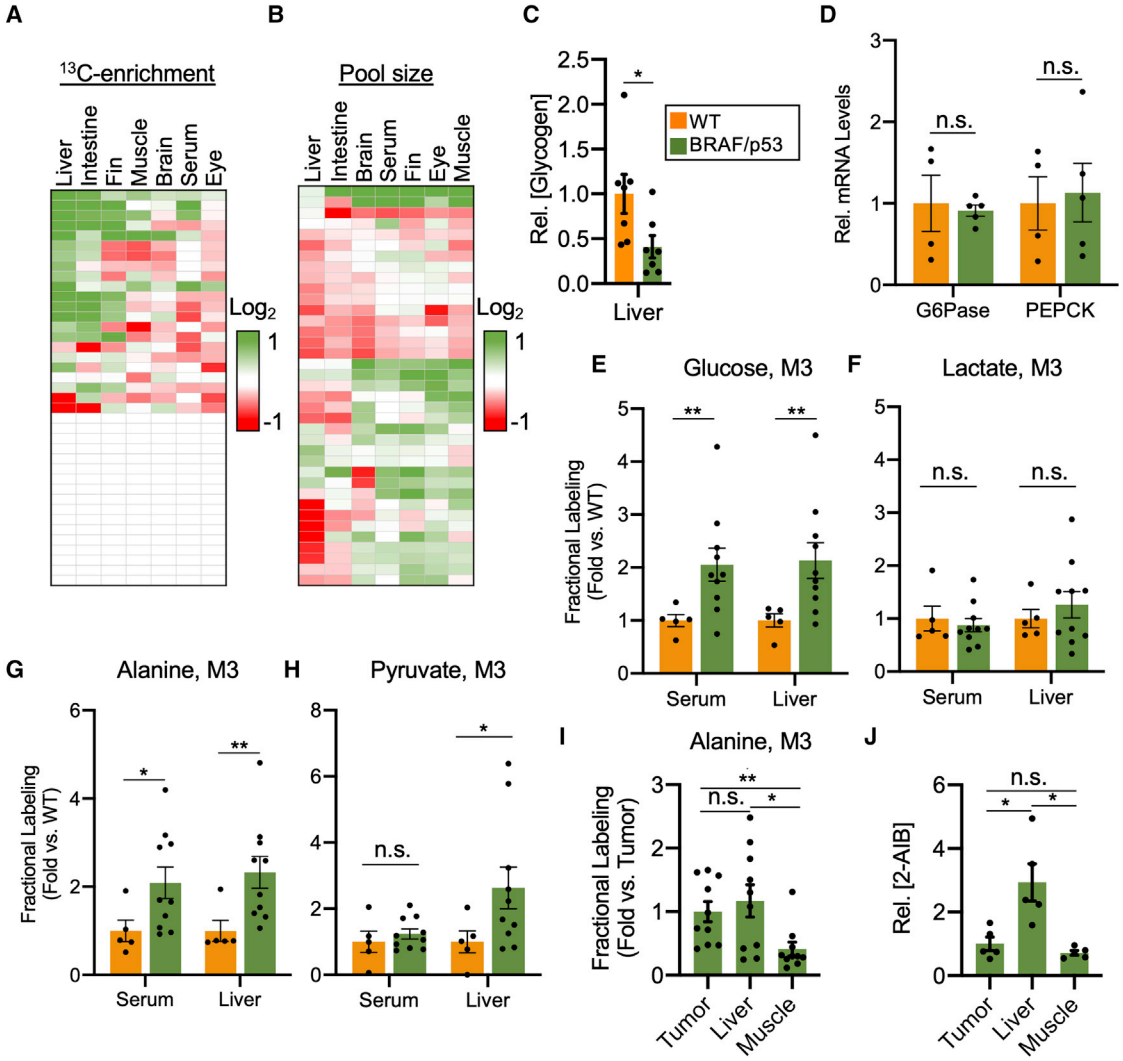

Figure 3. Systems-level isotope tracing reveals elevated hepatic gluconeogenesis in BRAF/p53 fish, fueled by melanoma-derived alanine

(A) Heatmap of normalized labeling differences in various metabolites from [U-^{13}C] glucose. Differences were calculated by comparing the normalized labeling of a tissue from BRAF/p53 fish with the normalized labeling of the same tissue from WT fish. Green indicates increased labeling and red indicates decreased labeling in metabolites from BRAF/p53 fish. Each data point represents the ratio of means from biological replicates. White boxes denote metabolites that did not incorporate ^{13}C tracer. n = 5–10 zebrafish per condition. The identities of each metabolite within the plot and full labeling data are available in Data S3.

(B) Heatmap of metabolite pool-size differences in tissues from BRAF/p53 fish relative to tissues from WT fish. Green indicates larger pool size, and red indicates smaller pool size of metabolites from BRAF/p53 fish. Each data point represents the ratio of means from biological replicates. n = 5–10 zebrafish per condition. The identities of each metabolite within the plot and pool-size data are available in Data S3.

(C) Relative concentration of hepatic glycogen in WT and BRAF/p53 fish, normalized to the WT group. Values are mean ± SEM; n = 7 zebrafish per condition.

(D) Relative expression of the hepatic gluconeogenic enzymes glucose 6-phosphatase (G6Pase) and phosphoenolpyruvate carboxykinase (PEPCK) in BRAF/p53 fish normalized to WT expression. Values are mean ± SEM; n = 4–5 zebrafish per group.

(E–H) Fractional labeling, relative to serum M6 glucose, of isotopologues for glucose (E), lactate (F), alanine (G), and pyruvate (H) in serum and liver of WT and BRAF/p53 animals. Data are presented as fold changes relative to the WT group. Values are mean ± SEM; n = 5–10 zebrafish per condition. Full labeling data are provided in Data S3.

(I) Fractional labeling, relative to serum M6 glucose, of alanine in tissues from BRAF/p53 animals. Data are presented as fold changes relative to alanine labeling in tumors. Values are mean ± SEM; n = 10 zebrafish per condition.

(J) Alanine uptake in tissues from BRAF/p53 zebrafish. Pool sizes of 2-aminoisobutyric acid (2-AIB) for tissues within a fish are normalized to the 2-AIB pool in its tumor. Values are mean ± SEM; n = 5 zebrafish per condition.

Statistically significant differences were assessed by a two-tailed paired t test and annotated as follows: *$p < 0.05$, **$p < 0.01$, or n.s. = not significant.

glutamine to tumor metabolism is minimal (Figure 2D). Thus, we focused our attention on the branched-chain amino acids (BCAAs). We placed BRAF/p53 zebrafish in water containing 2 mM [^{15}N] isoleucine, 2 mM [^{15}N] leucine, and 2 mM [^{15}N] valine for 24 h. The first step in BCAA degradation is transfer of the α-amino group to α-ketoglutarate to form glutamate through

Please cite this article in press as: Naser et al., Isotope tracing in adult zebrafish reveals alanine cycling between melanoma and liver, Cell Metabolism (2021), https://doi.org/10.1016/j.cmet.2021.04.014

CellPress

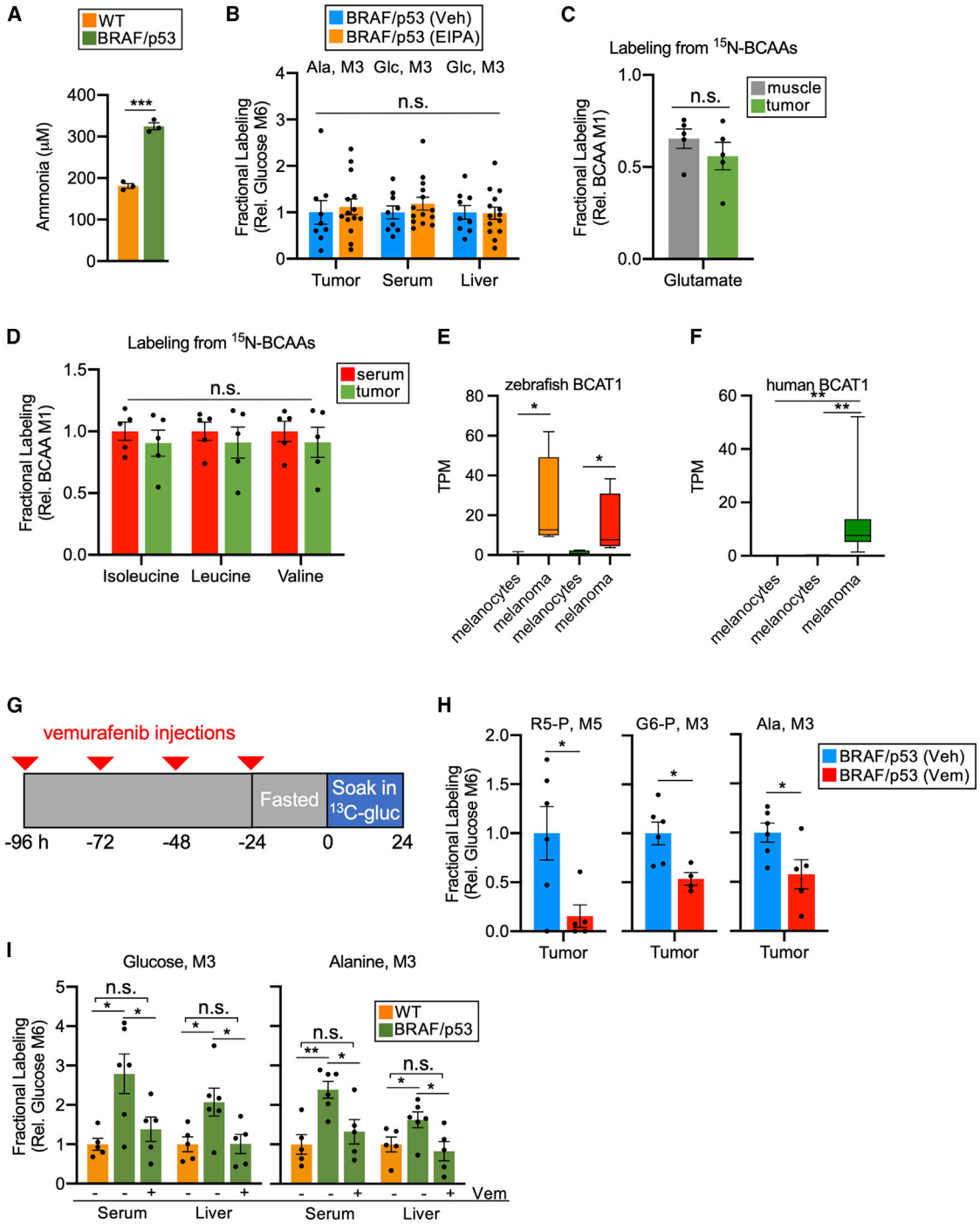

Figure 4. Circulating BCAAs provide melanoma with a source of nitrogen for the alanine cycle, which can be impaired by vemurafenib

(A) Concentration of ammonia excreted into tank water from WT and BRAF/p53 fish. Measurements were made 24 h after water refreshing. Each group was housed separately. Values are mean ± SEM; n = 3 zebrafish per condition.

(B) Fractional labeling, relative to M6 glucose, of M3 alanine and M3 glucose in BRAF/p53 zebrafish treated with EIPA or DMSO (Veh). Values are mean ± SEM; n = 9–14 zebrafish per condition.

(C) Fractional labeling, relative to serum M1 BCAAs, of glutamate in tumor and muscle of BRAF/p53 fish. Serum M1 BCAAs was determined by averaging the values of M1 from isoleucine, leucine, and valine. Data are available in Data S4. Values are mean ± SEM; n = 5 zebrafish.

(D) Fractional labeling, relative to serum M1 BCAAs, of isoleucine, leucine, and valine in serum and tumor of BRAF/p53 fish. Data are available in Data S4. Values are mean ± SEM; n = 5 zebrafish per condition.

(E) *BCAT1* expression in zebrafish melanocytes and BRAF/p53 melanoma cells. Our data are on the left, and data from Venkatesan et al. are on the right. Center line, median; box limits are first and third quartile; whiskers, range.

(legend continued on next page)

Please cite this article in press as: Naser et al., Isotope tracing in adult zebrafish reveals alanine cycling between melanoma and liver, Cell Metabolism (2021), https://doi.org/10.1016/j.cmet.2021.04.014

the activity of branched-chain amino acid aminotransferase (BCAT). The nitrogen can then be transferred to pyruvate by alanine aminotransferase (ALT), producing alanine for removal. Interestingly, free BCAAs taken up from the circulation contributed nearly 60% of the total nitrogen to glutamate in the tumor, suggesting that these amino acids are the largest donor of nitrogen to be removed from the tumor (Figure 4C). Additionally, the amount of glutamate labeled by [^{15}N] BCAAs was not significantly different than in muscle (Figure 4C). Muscle is known to be a main site of BCAA catabolism, which results in a surplus of nitrogen that is released into the circulation as alanine (Brosnan and Brosnan, 2006). These data further underscore that melanoma exhibit similar metabolism to muscle, taking up BCAAs and excreting their nitrogen via alanine. As further evidence that macropinocytosis is not a major contributor to the nitrogen pool in melanoma, we report that the labeling of BCAAs in the tumor is not significantly different than in serum (Figure 4D). This result is consistent with labeled BCAAs taken up by the tumor not being diluted by unlabeled BCAAs that result from the degradation of intact proteins.

To confirm that melanoma oncogenesis activates BCAA degradation, we compared expression of *branched-chain amino acid transferase 1* (*BCAT1*) in melanoma cells with normal melanocytes. We found that expression of *BCAT1* in zebrafish melanocytes was near zero. In contrast, expression was significantly upregulated in melanoma cells from BRAF/p53 tumors (Figure 4E). Our results are consistent with data from other zebrafish studies (Venkatesan et al., 2018). To determine the translational potential of our findings, we evaluated *BCAT1* expression in tumors obtained from a cohort of 18 patients with advanced melanoma treated at Washington University School of Medicine. Just as we observed in zebrafish, relative to healthy human melanocytes (Haltaufderhyde and Oancea, 2014; Reemann et al., 2014), *BCAT1* was highly expressed in melanoma (Figure 4F). These results suggest that BCAA catabolism is activated in melanoma from both a zebrafish model of disease and in human tumors.

Inhibiting BRAF^{V600E} with vemurafenib reduces tumor-liver alanine cycling

We next considered whether a selective inhibitor of BRAF^{V600E}, vemurafenib, affects tumor-liver alanine cycling. Vemurafenib is a clinically approved chemotherapy for melanoma expressing the *BRAF^{V600E}* mutation that has minimal toxicity and high tolerability in humans, mice, and zebrafish (Dang et al., 2016b; Kim and Cohen, 2016; Yang et al., 2010). On the basis of efficacy and toxicity profiles previously reported for zebrafish and murine melanoma models, we administered vemurafenib at 100 mg/kg/day via intraperitoneal injection to BRAF/p53 zebrafish (Dang et al., 2016b; Yang et al., 2010). After 4 days of consecutive vemurafenib or DMSO vehicle treatment, animals were transferred to new tanks containing 10 mM [U-^{13}C] glucose for 24 h prior to quantifying ammonia excretion and performing metabolomics (Figure 4G). After 4 days of drug treatment, no significant reduction in tumor size had occurred but a robust metabolic response was observed (Figure S4B). Compared with vehicle-treated BRAF/p53 fish, animals given vemurafenib for 4 days (1) excreted significantly less ammonia (Figure S4C); (2) incorporated less ^{13}C-label into central carbon metabolites in the tumor, with M3 labeling of alanine reduced by ~2-fold (Figures 4H, S4D, and S4E); and (3) showed a reduction in the pool size and ^{13}C-labeling of ribose 5-phosphate (R5-P), a nucleotide precursor whose production is upregulated in proliferating cells (Figures 4H and S4F) (Bruntz et al., 2017; Patra and Hay, 2014). Moreover, BRAF/p53 animals treated with vemurafenib for 4 days had levels of gluconeogenesis that were comparable to WT zebrafish, as indicated by M3 labeling in hepatic and circulating glucose (Figure 4I). In addition, no significant differences were observed in hepatic and circulating M3 alanine between BRAF/p53 animals treated with vemurafenib for 4 days and WT fish (Figure 4I). Collectively, these data show that inhibiting BRAF^{V600E} leads to the loss of alanine cycling between tumor and liver.

To better understand the effects of vemurafenib, we performed two additional experiments. First, we compared WT zebrafish administered vehicle and WT zebrafish administered vemurafenib at 100 mg/kg/day for 4 consecutive days. Following vehicle or vemurafenib treatment, the animals were transferred to tank water containing [U-^{13}C] glucose for 24 h. No differences in ^{13}C-labeling were found in metabolites from the circulation, liver, or muscle (Figures S5A–S5F). These data indicate that vemurafenib does not affect alanine cycling in the absence of BRAF^{V600E}. Second, we performed the same experiments outlined above with vemurafenib, but we administered the drug for 10 consecutive days at 100 mg/kg/day. After 10 days of treating BRAF/p53 zebrafish with vemurafenib, tumors were reduced in size by >95% (Figures S5G and S5H). Yet ammonia excretion after 10 days of vemurafenib treatment was not significantly different from ammonia excretion after 4 days of vemurafenib treatment (Figure S4C). Isotope-tracing data from animals treated with vemurafenib for 4 and 10 days were also comparable (Figure S5I). These results indicate that alanine cycling is not reduced in BRAF/p53 zebrafish due to tumor regression, but instead results from the inhibition of BRAF^{V600E} signaling.

(F) *BCAT1* expression in human melanocytes and human melanoma. Data on left are from Haltaufderhyde et al., data in center are from Reeman et al., and our data are on right.

(G) Schematic of when vemurafenib and [U-^{13}C] glucose were administered to melanoma-bearing zebrafish. Red triangles denote the timing of vemurafenib injections.

(H) Fractional labeling, relative to serum M6 glucose, of the central carbon intermediates ribose 5-phosphate (left), glucose 6-phosphate (middle), and alanine (right) in tumors treated with either DMSO (Veh) or vemurafenib (Vem). Data are normalized to the vehicle-treated group. Full labeling data are provided in Data S4. Values are mean ± SEM; n = 4–6 zebrafish per condition.

(I) Fractional labeling, relative to serum M6 glucose, of gluconeogenesis-derived glucose (left) and alanine (right) in circulation and liver of vehicle-treated WT, vehicle-treated BRAF/p53, and vemurafenib-treated BRAF/p53 fish. Data are normalized to the vehicle-treated WT group. Values are mean ± SEM; n = 5–6 zebrafish per condition. Full labeling data are provided in Data S4.

Statistically significant differences were assessed by a two-tailed paired t test (A–D, H, and I) or a Wilcoxon rank-sum test (E and F) and annotated as follows: *p < 0.05, **p < 0.01, ***p < 0.001, or n.s. = not significant. R5-P, ribose 5-phosphate; G6-P, glucose 6-phosphate; Ala, alanine; Glc, glucose.

Please cite this article in press as: Naser et al., Isotope tracing in adult zebrafish reveals alanine cycling between melanoma and liver, Cell Metabolism (2021), https://doi.org/10.1016/j.cmet.2021.04.014

Inhibiting ALT reduces BCAA catabolism, alanine cycling, and tumor volume

Our observations suggest that activating BCAA degradation in melanoma results in excess nitrogen, which is released from the tumor via alanine and then transported to the liver for removal as ammonia. Thus, we sought to evaluate whether inhibiting alanine production in melanoma influences BCAA catabolism and subsequent tumor growth. First, we treated melanoma-bearing zebrafish with an ALT inhibitor (β-chloroalanine) for 10 days. Next, we transferred the animals to tank water containing [U-^{13}C] BCAAs for 24 h. Given that BCAAs enter the TCA cycle as acetyl-CoA and propionyl-CoA following the removal of their α-amino group, which ultimately is transferred to pyruvate via ALT (Figure 5A), we assessed the contribution that BCAAs made to the TCA cycle in tumors. Inhibiting ALT with β-chloroalanine significantly reduced the contribution that [U-^{13}C] BCAAs made to the TCA cycle (Figure 5B). Furthermore, ALT inhibition led to an accumulation of BCAAs in serum, an accumulation of BCAAs in tumor, decreased levels of circulating glucose, and decreased levels of alanine in tumor, serum, and liver (Figure 5C). Reducing oxidation of BCAAs and alanine production in melanoma also correlated with a 50% reduction in tumor size (Figures 5D and 5E). Together, our results indicate that BCAA catabolism contributes to tumor growth and that removal of nitrogen from the tumor via alanine is required for efficient use of these substrates by melanoma.

CONCLUSION

In summary, the work presented here establishes the adult zebrafish as a well-suited model organism to study whole-body physiology with isotope-tracer analysis and metabolomics. The experimental procedures we have introduced can be easily adapted to study any zebrafish model of disease (Lieschke and Currie, 2007; Salmi et al., 2019; Seth et al., 2013). Using a BRAF/p53 model of melanoma, we have shown that the presence of a tumor leads to systemic alterations in metabolism. In particular, our results demonstrate that the liver uses tumor-excreted alanine as a substrate for gluconeogenesis. The process maintains circulating glucose levels and helps support the high glycolytic demands of the tumor. While a tumor-liver alanine cycle has been proposed before (DeBerardinis and Cheng, 2010), to the best of our knowledge, this is the first time that it has been directly demonstrated *in vivo*. In melanoma, we show that the cycle supports the removal of excess nitrogen from the tumor obtained from increased catabolism of BCAAs and that blocking the cycle with an inhibitor of ALT may be an attractive treatment. Our work underscores the importance of metabolic cooperation between the tumor and otherwise healthy tissues in an organism, providing an example of how tumors can exploit the normal physiology of the host for its own benefits. Characterizing such interactions has the potential to reveal new metabolic opportunities for therapeutic intervention associated with distal, non-malignant tissues rather than the tumor itself.

Limitations of study

We report that the presence of a tumor alters the metabolism of multiple non-cancerous tissues such as liver, intestine, muscle, and brain in a zebrafish model of melanoma. Here, we focused on characterizing changes that are associated with a tumor-liver alanine cycle. Further investigation is needed to understand the nature of other metabolic interactions, how they may influence melanoma growth, and whether similar changes are observed with different types of tumors. Using our zebrafish model of melanoma, we studied two independent therapeutic approaches. The first, vemurafenib, is a well-established inhibitor of BRAF^{V600E}. Vemurafenib reduced alanine cycling between melanoma and liver 4 days after the start of treatment, before any significant decrease in tumor volume had occurred. The reduction in alanine cycling persisted after 10 days of treatment, when tumor volume had decreased by >95%. Vemurafenib does not directly target alanine or BCAA metabolism in the tumor, but a network of BRAF-regulated transcription factors controlling glycolysis have been identified in melanoma cells (Parmenter et al., 2014). Additional studies are required to link BRAF^{V600E} inhibition in tumors with downstream changes in alanine and BCAA metabolism. The second therapeutic we evaluated, β-chloroalanine, was selected because it directly inhibits the ALT enzyme involved in the alanine cycle. After 10 days of treatment, β-chloroalanine reduced tumor volume by 50%. We demonstrated that β-chloroalanine acts by impairing alanine production and oxidation of BCAAs in the tumor, thereby reducing tumor-liver alanine cycling. More work is needed, however, to determine the extent that inhibiting ALT in the liver also reduces alanine cycling and tumor burden.

STAR★METHODS

Detailed methods are provided in the online version of this paper and include the following:

- KEY RESOURCES TABLE
- RESOURCE AVAILABILITY
  - Lead contact
  - Materials availability
  - Data and code availability
- EXPERIMENTAL MODEL AND SUBJECT DETAILS
  - Zebrafish husbandry
  - Serum harvest
- METHOD DETAILS
  - Isotope tracing
  - Metabolite extraction
  - LC-MS analysis
  - Analysis of liver weight
  - Ammonia excretion assay
  - Glycogen assay
  - Vemurafenib treatment
  - EIPA treatment
  - 2-deoxyglucose and 2-aminoisobutyric acid assay
  - ß-chloroalanine treatment
  - Histology
  - Real-time PCR analysis
  - Analysis of BCAT1 expression in zebrafish
  - Analysis of BCAT1 expression in human patients
- QUANTIFICATION AND STATISTICAL ANALYSIS
  - Data analysis

Please cite this article in press as: Naser et al., Isotope tracing in adult zebrafish reveals alanine cycling between melanoma and liver, Cell Metabolism (2021), https://doi.org/10.1016/j.cmet.2021.04.014

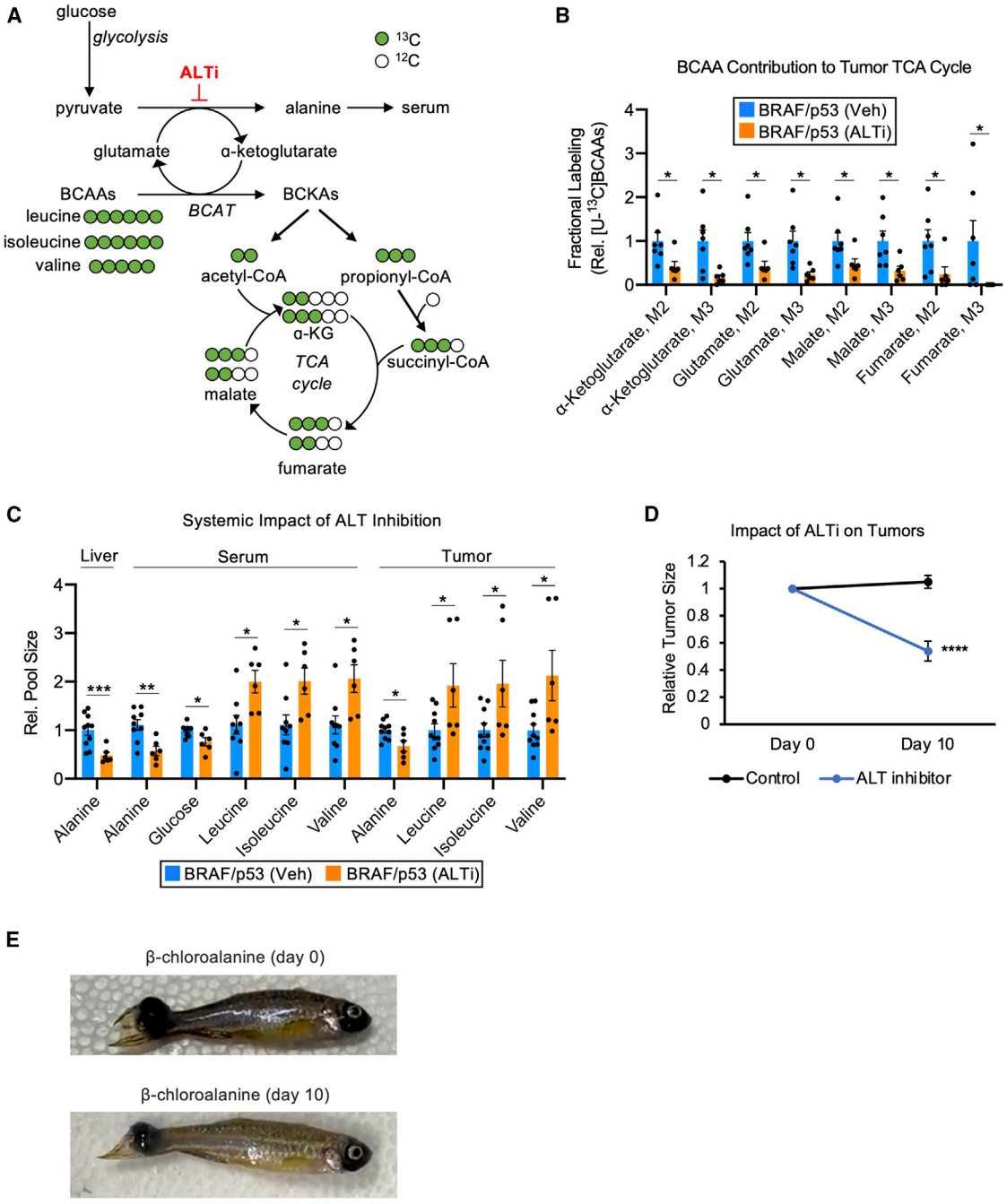

Figure 5. Pharmacologically inhibiting ALT provides direct support for tumor-liver alanine cycling

(A) Schematic to illustrate the transformation of BCAA carbon to key intermediates in central carbon metabolism.

(B) Fractional labeling, relative to serum [U-^{13}C] BCAAs, of the central carbon intermediates α-ketoglutarate, glutamate, malate, and fumarate in tumors treated with either vehicle (Veh) or β-chloroalanine (ALTi). Data are normalized to the vehicle-treated group. Serum [U-^{13}C] BCAAs was determined by averaging [U-^{13}C] isoleucine, [U-^{13}C] leucine, and [U-^{13}C] valine. Values are mean ± SEM; n = 6–7 zebrafish per condition. Full labeling data are available in Data S5.

(C) Relative pool sizes of central carbon metabolites from BRAF/p53 animals treated with either vehicle (Veh) or β-chloroalanine (ALTi). Data are normalized to the vehicle-treated group. Values are mean ± SEM; n = 6–10 zebrafish per condition. Data are available in Data S5.

(D) Relative change from baseline in tumor volume after 10 days of β-chloroalanine (ALT inhibitor) treatment. Values are mean ± SEM; n = 9–10 tumors per condition. Tumor dimensions are included Data S5.

(E) Representative image of tumor regression in a BRAF/p53 fish after 10 days of β-chloroalanine treatment.

Statistically significant differences were assessed by a two-tailed paired t test and annotated as follows: *p < 0.05, **p < 0.01, ***p < 0.001, ****p < 0.0001, or n.s. = not significant.

SUPPLEMENTAL INFORMATION

Supplemental information can be found online at https://doi.org/10.1016/j.cmet.2021.04.014.

ACKNOWLEDGMENTS

Financial support was received for this work from NIH awards R35ES028365 (G.J.P.), U01CA235482 (G.J.P.), and R24OD024624 (G.J.P.) as well as the Edward Mallinckrodt, Jr. Foundation (G.J.P.) and the Pew Charitable Trusts (G.J.P.). We dedicate this work to the late Stephen L. Johnson, who was an inspiring mentor to the co-authors. His collaborative generosity was essential to carrying out these studies. The authors thank Wandy Beatty of the Molecular Microbiology Imaging Facility for assistance with periodic acid-Schiff (PAS) imaging.

AUTHOR CONTRIBUTIONS

F.J.N., M.M.J., and G.J.P. designed the study. F.J.N., M.M.J., R.F.-G., J.L.S., S.L.J., and G.J.P. contributed to the development of the zebrafish-metabolomics workflow. F.J.N. and M.M.J. performed all zebrafish experiments. F.J.N., M.M.J., and J.L.S. bred and maintained animals. K.C. and E.S. contributed to data processing and data analysis. S.R.D. performed tissue slicing. E.T.K. and C.K.K. performed expression analysis for zebrafish specimens. L.Y., B.K., L.D., and R.C.F. performed expression analysis for human melanoma. F.J.N., M.M.J., L.P.S., and G.J.P. wrote the manuscript. All authors discussed the results, contributed to data interpretation, and commented on the manuscript.

DECLARATION OF INTERESTS

G.J.P. is a scientific advisory board member for Cambridge Isotope Laboratories.

Received: July 21, 2020
Revised: February 8, 2021
Accepted: April 19, 2021
Published: May 13, 2021

REFERENCES

Akedo, H., and Christensen, H.N. (1962). Transfer of amino acids across the intestine: a new model amino acid. J. Biol. Chem. *237*, 113–117.

Babaei, F., Ramalingam, R., Tavendale, A., Liang, Y., Yan, L.S., Ajuh, P., Cheng, S.H., and Lam, Y.W. (2013). Novel blood collection method allows plasma proteome analysis from single zebrafish. J. Proteome Res. *12*, 1580–1590.

Bonjorn, V.M., Latour, M.G., Bélanger, P., and Lavoie, J.M. (2002). Influence of prior exercise and liver glycogen content on the sensitivity of the liver to glucagon. J. Appl. Physiol. *92*, 188–194.

Braun, M.H., Steele, S.L., and Perry, S.F. (2009). The responses of zebrafish (Danio rerio) to high external ammonia and urea transporter inhibition: nitrogen excretion and expression of rhesus glycoproteins and urea transporter proteins. J. Exp. Biol. *212*, 3846–3856.

Bray, N.L., Pimentel, H., Melsted, P., and Pachter, L. (2016). Near-optimal probabilistic RNA-seq quantification. Nat. Biotechnol. *34*, 525–527.

Brosnan, J.T., and Brosnan, M.E. (2006). Branched-chain amino acids: enzyme and substrate regulation. J. Nutr. *136* (*Supplement*), 207S–211S.

Bruntz, R.C., Lane, A.N., Higashi, R.M., and Fan, T.W. (2017). Exploring cancer metabolism using stable isotope-resolved metabolomics (SIRM). J. Biol. Chem. *292*, 11601–11609.

Buescher, J.M., Antoniewicz, M.R., Boros, L.G., Burgess, S.C., Brunengraber, H., Clish, C.B., DeBerardinis, R.J., Feron, O., Frezza, C., Ghesquiere, B., et al. (2015). A roadmap for interpreting (13)C metabolite labeling patterns from cells. Curr. Opin. Biotechnol. *34*, 189–201.

Chen, Y.J., Mahieu, N.G., Huang, X., Singh, M., Crawford, P.A., Johnson, S.L., Gross, R.W., Schaefer, J., and Patti, G.J. (2016). Lactate metabolism is associated with mammalian mitochondria. Nat. Chem. Biol. *12*, 937–943.

Dang, M., Fogley, R., and Zon, L.I. (2016a). Identifying novel cancer therapies using chemical genetics and zebrafish. Adv. Exp. Med. Biol. *916*, 103–124.

Dang, M., Henderson, R.E., Garraway, L.A., and Zon, L.I. (2016b). Long-term drug administration in the adult zebrafish using oral gavage for cancer preclinical studies. Dis. Model. Mech. *9*, 811–820.

Davidson, S.M., Papagiannakopoulos, T., Olenchock, B.A., Heyman, J.E., Keibler, M.A., Luengo, A., Bauer, M.R., Jha, A.K., O'Brien, J.P., Pierce, K.A., et al. (2016). Environment impacts the metabolic dependencies of Ras-driven non-small cell lung cancer. Cell Metab *23*, 517–528.

Davidson, S.M., Jonas, O., Keibler, M.A., Hou, H.W., Luengo, A., Mayers, J.R., Wyckoff, J., Del Rosario, A.M., Whitman, M., Chin, C.R., et al. (2017). Direct evidence for cancer-cell-autonomous extracellular protein catabolism in pancreatic tumors. Nat. Med. *23*, 235–241.

DeBerardinis, R.J., and Chandel, N.S. (2016). Fundamentals of cancer metabolism. Sci. Adv. *2*, e1600200.

DeBerardinis, R.J., and Cheng, T. (2010). Q's next: the diverse functions of glutamine in metabolism, cell biology and cancer. Oncogene *29*, 313–324.

DeBerardinis, R.J., Mancuso, A., Daikhin, E., Nissim, I., Yudkoff, M., Wehrli, S., and Thompson, C.B. (2007). Beyond aerobic glycolysis: transformed cells can engage in glutamine metabolism that exceeds the requirement for protein and nucleotide synthesis. Proc. Natl. Acad. Sci. USA *104*, 19345–19350.

Dymowska, A.K., Boyle, D., Schultz, A.G., and Goss, G.G. (2015). The role of acid-sensing ion channels in epithelial Na+ uptake in adult zebrafish (Danio rerio). J. Exp. Biol. *218*, 1244–1251.

Eames, S.C., Philipson, L.H., Prince, V.E., and Kinkel, M.D. (2010). Blood sugar measurement in zebrafish reveals dynamics of glucose homeostasis. Zebrafish *7*, 205–213.

Edmondson, J.W., Lumeng, L., and Li, T.K. (1979). Comparative studies of alanine and alpha-aminoisobutyric acid uptake by freshly isolated rat liver cells. J. Biol. Chem. *254*, 1653–1658.

Faubert, B., Li, K.Y., Cai, L., Hensley, C.T., Kim, J., Zacharias, L.G., Yang, C., Do, Q.N., Doucette, S., Burguete, D., et al. (2017). Lactate metabolism in human lung tumors. Cell *171*, 358–371.e9.

Felig, P. (1973). The glucose-alanine cycle. Metabolism *22*, 179–207.

Fernández-García, J., Altea-Manzano, P., Pranzini, E., and Fendt, S.M. (2020). Stable isotopes for tracing mammalian-cell metabolism in vivo. Trends Biochem. Sci. *45*, 185–201.

Gao, X., Sanderson, S.M., Dai, Z., Reid, M.A., Cooper, D.E., Lu, M., Richie, J.P., Jr., Ciccarella, A., Calcagnotto, A., Mikhael, P.G., et al. (2019). Dietary methionine influences therapy in mouse cancer models and alters human metabolism. Nature *572*, 397–401.

Haltaufderhyde, K.D., and Oancea, E. (2014). Genome-wide transcriptome analysis of human epidermal melanocytes. Genomics *104*, 482–489.

Haüssinger, D. (1990). Nitrogen metabolism in liver: structural and functional organization and physiological relevance. Biochem. J. *267*, 281–290.

Hensley, C.T., Faubert, B., Yuan, Q., Lev-Cohain, N., Jin, E., Kim, J., Jiang, L., Ko, B., Skelton, R., Loudat, L., et al. (2016). Metabolic heterogeneity in human lung tumors. Cell *164*, 681–694.

Hsiao, J.J., Potter, O.G., Chu, T.W., and Yin, H. (2018). Improved LC/MS methods for the analysis of metal-sensitive analytes using medronic acid as a mobile phase additive. Anal. Chem. *90*, 9457–9464.

Hui, S., Ghergurovich, J.M., Morscher, R.J., Jang, C., Teng, X., Lu, W., Esparza, L.A., Reya, T., Le Zhan, Z., Yanxiang Guo, J., et al. (2017). Glucose feeds the TCA cycle via circulating lactate. Nature *551*, 115–118.

Jain, M., Nilsson, R., Sharma, S., Madhusudhan, N., Kitami, T., Souza, A.L., Kafri, R., Kirschner, M.W., Clish, C.B., and Mootha, V.K. (2012). Metabolite profiling identifies a key role for glycine in rapid cancer cell proliferation. Science *336*, 1040–1044.

Jang, C., Hui, S., Zeng, X., Cowan, A.J., Wang, L., Chen, L., Morscher, R.J., Reyes, J., Frezza, C., Hwang, H.Y., et al. (2019). Metabolite exchange between mammalian organs quantified in pigs. Cell Metab *30*, 594–606.e3.

Kamphorst, J.J., Cross, J.R., Fan, J., de Stanchina, E., Mathew, R., White, E.P., Thompson, C.B., and Rabinowitz, J.D. (2013). Hypoxic and Ras-transformed cells support growth by scavenging unsaturated fatty acids from lysophospholipids. Proc. Natl. Acad. Sci. USA *110*, 8882–8887.

Kim, A., and Cohen, M.S. (2016). The discovery of vemurafenib for the treatment of BRAF-mutated metastatic melanoma. Expert Opin. Drug Discov. *11*, 907–916.

Kinkel, M.D., Eames, S.C., Philipson, L.H., and Prince, V.E. (2010). Intraperitoneal injection into adult zebrafish. J. Vis. Exp. *42*, 2126.

Krall, A.S., Xu, S., Graeber, T.G., Braas, D., and Christofk, H.R. (2016). Asparagine promotes cancer cell proliferation through use as an amino acid exchange factor. Nat. Commun. *7*, 11457.

Li, J.M., Li, L.Y., Qin, X., Ning, L.J., Lu, D.L., Li, D.L., Zhang, M.L., Wang, X., and Du, Z.Y. (2017). Systemic regulation of L-carnitine in nutritional metabolism in zebrafish, Danio rerio. Sci. Rep. *7*, 40815.

Lieschke, G.J., and Currie, P.D. (2007). Animal models of human disease: zebrafish swim into view. Nat. Rev. Genet. *8*, 353–367.

Nechiporuk, A., Finney, J.E., Keating, M.T., and Johnson, S.L. (1999). Assessment of polymorphism in zebrafish mapping strains. Genome Res *9*, 1231–1238.

Parmenter, T.J., Kleinschmidt, M., Kinross, K.M., Bond, S.T., Li, J., Kaadige, M.R., Rao, A., Sheppard, K.E., Hugo, W., Pupo, G.M., et al. (2014). Response of BRAF-mutant melanoma to BRAF inhibition is mediated by a network of transcriptional regulators of glycolysis. Cancer Discov *4*, 423–433.

Patra, K.C., and Hay, N. (2014). The pentose phosphate pathway and cancer. Trends Biochem. Sci. *39*, 347–354.

Patton, E.E., Widlund, H.R., Kutok, J.L., Kopani, K.R., Amatruda, J.F., Murphey, R.D., Berghmans, S., Mayhall, E.A., Traver, D., Fletcher, C.D.M., et al. (2005). BRAF mutations are sufficient to promote nevi formation and cooperate with p53 in the genesis of melanoma. Curr. Biol. *15*, 249–254.

Pedroso, G.L., Hammes, T.O., Escobar, T.D., Fracasso, L.B., Forgiarini, L.F., and da Silveira, T.R. (2012). Blood collection for biochemical analysis in adult zebrafish. J. Vis. Exp. *63*, e3865.

Randall, D.J., and Wright, P.A. (1987). Ammonia distribution and excretion in fish. Fish Physiol. Biochem. *3*, 107–120.

Ratnikov, B., Aza-Blanc, P., Ronai, Z.A., Smith, J.W., Osterman, A.L., and Scott, D.A. (2015). Glutamate and asparagine cataplerosis underlie glutamine addiction in melanoma. Oncotarget *6*, 7379–7389.

Ratnikov, B.I., Scott, D.A., Osterman, A.L., Smith, J.W., and Ronai, Z.A. (2017). Metabolic rewiring in melanoma. Oncogene *36*, 147–157.

Reemann, P., Reimann, E., Ilmjärv, S., Porosaar, O., Silm, H., Jaks, V., Vasar, E., Kingo, K., and Kõks, S. (2014). Melanocytes in the skin–comparative whole transcriptome analysis of main skin cell types. PLoS One *9*, e115717.

Ross, B.D., Hems, R., and Krebs, H.A. (1967). The rate of gluconeogenesis from various precursors in the perfused rat liver. Biochem. J. *102*, 942–951.

Salmi, T.M., Tan, V.W.T., and Cox, A.G. (2019). Dissecting metabolism using zebrafish models of disease. Biochem. Soc. Trans. *47*, 305–315.

Scott, D.A., Richardson, A.D., Filipp, F.V., Knutzen, C.A., Chiang, G.G., Ronai, Z.A., Osterman, A.L., and Smith, J.W. (2011). Comparative metabolic flux profiling of melanoma cell lines: beyond the Warburg effect. J. Biol. Chem. *286*, 42626–42634.

Seth, A., Stemple, D.L., and Barroso, I. (2013). The emerging use of zebrafish to model metabolic disease. Dis. Model. Mech. *6*, 1080–1088.

Spalding, J.L., Naser, F.J., Mahieu, N.G., Johnson, S.L., and Patti, G.J. (2018). Trace phosphate improves ZIC-pHILIC peak shape, sensitivity, and coverage for untargeted metabolomics. J. Proteome Res. *17*, 3537–3546.

Spinelli, J.B., Kelley, L.P., and Haigis, M.C. (2017). An LC-MS approach to quantitative measurement of ammonia isotopologues. Sci. Rep. *7*, 10304.

Su, X., Lu, W., and Rabinowitz, J.D. (2017). Metabolite spectral accuracy on orbitraps. Anal. Chem. *89*, 5940–5948.

Truong, L., Reif, D.M., St Mary, L., Geier, M.C., Truong, H.D., and Tanguay, R.L. (2014). Multidimensional in vivo hazard assessment using zebrafish. Toxicol. Sci. *137*, 212–233.

Vander Heiden, M.G., and DeBerardinis, R.J. (2017). Understanding the intersections between metabolism and cancer biology. Cell *168*, 657–669.

Vander Heiden, M.G., Cantley, L.C., and Thompson, C.B. (2009). Understanding the Warburg effect: the metabolic requirements of cell proliferation. Science *324*, 1029–1033.

Venkatesan, A.M., Vyas, R., Gramann, A.K., Dresser, K., Gujja, S., Bhatnagar, S., Chhangawala, S., Gomes, C.B.F., Xi, H.S., Lian, C.G., et al. (2018). Ligand-activated BMP signaling inhibits cell differentiation and death to promote melanoma. J. Clin. Invest. *128*, 294–308.

Westerfield, M. (2000). The Zebrafish Book. A Guide for the Laboratory Use of Zebrafish (Danio rerio), Fourth Edition (University of Oregon Press).

White, R., Rose, K., and Zon, L. (2013). Zebrafish cancer: the state of the art and the path forward. Nat. Rev. Cancer *13*, 624–636.

Yang, H., Higgins, B., Kolinsky, K., Packman, K., Go, Z., Iyer, R., Kolis, S., Zhao, S., Lee, R., Grippo, J.F., et al. (2010). RG7204 (PLX4032), a selective BRAFV600E inhibitor, displays potent antitumor activity in preclinical melanoma models. Cancer Res *70*, 5518–5527.

Yao, C.H., Fowle-Grider, R., Mahieu, N.G., Liu, G.Y., Chen, Y.J., Wang, R., Singh, M., Potter, G.S., Gross, R.W., Schaefer, J., et al. (2016). Exogenous fatty acids are the preferred source of membrane lipids in proliferating fibroblasts. Cell Chem. Biol. *23*, 483–493.

Zang, L., Maddison, L.A., and Chen, W. (2018). Zebrafish as a model for obesity and diabetes. Front. Cell Dev. Biol. *6*, 91.

Please cite this article in press as: Naser et al., Isotope tracing in adult zebrafish reveals alanine cycling between melanoma and liver, Cell Metabolism (2021), https://doi.org/10.1016/j.cmet.2021.04.014

CellPress

STAR★METHODS

KEY RESOURCES TABLE

REAGENT or RESOURCE	SOURCE	IDENTIFIER
Biological samples		
Resected human melanoma tumors	This paper	N/A
Chemicals, peptides, and recombinant proteins		
[U-^{13}C] glucose	Cambridge Isotopes	Cat#CLM-1396-PK
[U-^{13}C] glutamine	Cambridge Isotopes	Cat#CLM-1822-PK
[^{15}N] valine	Cambridge Isotopes	Cat#NLM-316-PK
[^{15}N] leucine	Cambridge Isotopes	Cat#NLM-142-PK
[^{15}N] isoleucine	Cambridge Isotopes	Cat#NLM-292-PK
[U-^{13}C] valine	Cambridge Isotopes	Cat#CLM-2249-PK
[U-^{13}C] leucine	Cambridge Isotopes	Cat#CLM-2262-PK
[U-^{13}C] isoleucine	Cambridge Isotopes	Cat#CLM-2248-PK
Penicillin-Streptomycin (10,000 U/mL)	Life Technologies	Cat#15140122
Vemurafenib	Selleckchem	Cat#S1267
Tricaine-S (MS-222)	Western Chemical	Cat#ANADA200-226
5-(N-ethyl-N-isopropyl)amiloride (EIPA)	Sigma	Cat#A3085
Dimethyl sulfoxide (DMSO)	Sigma	Cat#PHR1309
2-aminoisobutyric acid (2-AIB)	Sigma	Cat#850993
2-deoxy-D-glucose (2-DG)	Sigma	Cat#D8375
2-deoxyglucose 6-phosphate	Sigma	Cat#SMB00932
ß-chloro-L-alanine hydrochloride	Sigma	Cat#C9033
Critical commercial assays		
Glycogen Assay Kit	Abcam	Cat#ab65620
Bradford reagent	Bio-Rad	Cat#5000006
SuperScript III First-Strand Synthesis SuperMix	Invitrogen	Cat#18080400
SuperScript II Reverse Transcriptase	Invitrogen	Cat#18064014
PowerUp SYBR Green Master Mix	Applied Biosystems	Cat#A25918
Macherey Nagel Nucleospin XS kit	Fischer Scientific	Cat#NC0389511
RNeasy Mini Kit	Qiagen	Cat#74104
Periodic acid-Schiff (PAS) Kit	Sigma	Cat#395B-1KT
Experimental models: Organisms/strains		
D. rerio: adult sjA	Nechiporuk et al., 1999	N/A
D rerio: adult BRAF/p53	Patton et al., 2005	N/A
Oligonucleotides		
EF1α Forward Primer: CCCCTGGACACAGAGACTTCATC	Li et al., 2017	GenBank No. L23807.1
EF1α Reverse Primer: ATACCAGCCTCAAACTCACCGAC	Li et al., 2017	GenBank No. L23807.1
β-actin Forward Primer: TCTGGTGATGGTGTGACCCA	Li et al., 2017	GenBank No. AY222742
β-actin Reverse Primer: GGTGAAGCTGTAGCCACGCT	Li et al., 2017	GenBank No. AY222742
G6Pase Forward Primer: TGGCAGTGATAGGAGATTGGCTT	Li et al., 2017	GenBank No. BC148168.1
G6Pase Reverse Primer: AGTAGGACGTCTCATGGACCCAC	Li et al., 2017	GenBank No. BC148168.1

(*Continued on next page*)

Please cite this article in press as: Naser et al., Isotope tracing in adult zebrafish reveals alanine cycling between melanoma and liver, Cell Metabolism (2021), https://doi.org/10.1016/j.cmet.2021.04.014

Continued

REAGENT or RESOURCE	SOURCE	IDENTIFIER
PEPCK Forward Primer: ATCGCATCACGCATCGCTAAA	Li et al., 2017	GenBank No. NM_214751
PEPCK Reverse Primer: CCGCTGCGAAATACTTCTTCTGT	Li et al., 2017	GenBank No. NM_214751
Software and algorithms		
Skyline	University of Washington	https://skyline.ms/project/home/begin.view?
Compound Discoverer 3.0	Thermo Scientific	N/A
GraphPad Prism 7	GraphPad Software	https://www.graphpad.com/
Other		
NanoFil 10 μL syringe	World Precision Instruments	Cat#NANOFIL
35G beveled NanoFil needle	World Precision Instruments	Cat#NF35BV-2
Disposable Pellet Pestle	Axygen	Cat#PES-15-B-SI
SeQuant ZIC-pHILIC guard column	EMD Millipore	Cat#150437
SeQuant ZIC-pHILIC column	EMD Millipore	Cat#150462

RESOURCE AVAILABILITY

Lead contact

Further information and requests for resources and reagents should be directed to and will be fulfilled by the Lead Contact, Gary Patti (gjpattij@wustl.edu).

Materials availability

This study did not generate new unique reagents.

Data and code availability

The published article includes all datasets generated or analyzed in this study.

EXPERIMENTAL MODEL AND SUBJECT DETAILS

Zebrafish husbandry

This study was carried out in accordance with the Washington University Institutional Animal Care and Use Committee (IACUC) regulations. Wild-type (WT) fish were inbred AB strain (sjA) (Nechiporuk et al., 1999). *p53*$^{-/-}$ and transgenic *mitfa-BRAF*^{V600E} lines were crossed to produce melanoma-bearing fish (referred to as BRAF/p53), as previously described (Patton et al., 2005). All fish were reared according to standard laboratory procedures (Westerfield, 2000). Fish were kept in an indoor environment at a temperature of 28 ± 1 °C with a 14:10-h light:dark circadian cycle. Both female and male fish were used for experiments at random. Experiments were conducted with adult, age-matched animals. To assay tumor growth, melanoma dimensions were measured by using digital calipers. Tumor size was approximated as the volume of a half ellipsoid, $\frac{2}{3}\pi abc$, where a, b, and c represent the radii of tumor length, width, and height respectively.

To anesthetize by gradual cooling, zebrafish were initially placed in a beaker containing 100 mL of water at 17 °C. The beaker containing the fish was then placed in a shallow ice bath to allow for gradual cooling over the course of 5 min down to 12 °C until stage III, phase 2 anesthesia was achieved, characterized by loss of reactivity, loss of balance, and loss of operculum movements. For experiments testing tricaine anesthesia, fish were immersed in 0.02% MS-222 in facility water for 1 – 2 min until stage III, phase 2 anesthesia was achieved. Euthanasia was performed by placing fish in an ice-water slurry for at least 10 min and was deemed complete 1 min after the cessation of opercular movements.

Serum harvest

For blood collection method development, we evaluated two protocols. First, blood was pipetted directly from a zebrafish following wound generation as previously described (Pedroso et al., 2012). Briefly, an anesthetized zebrafish was removed from water and dried thoroughly with a Kimwipe. A razor blade was used to amputate the caudal fin and some associated distal tissue by making a transverse cross section midway between the anal and caudal fin. Upon caudal fin amputation, blood was pipetted directly from the wound, with particular focus on the dorsal aorta region, using tips of various sizes.

To evaluate a second protocol that employed low-speed centrifugation, a simple blood-collection device was prepared by forming a small hole in the bottom of a 1.5 mL microcentrifuge tube (the holding tube) with a razor blade. The hole was approximately the

Please cite this article in press as: Naser et al., Isotope tracing in adult zebrafish reveals alanine cycling between melanoma and liver, Cell Metabolism (2021), https://doi.org/10.1016/j.cmet.2021.04.014

diameter of the cross section created via caudal fin amputation (~0.5 mm). The holding tube was fit into a 0.5 mL microcentrifuge tube (the collection tube) and secured with adhesive. The holding tube attached to the collection tube constituted the blood-collection apparatus. To collect blood, zebrafish were anesthetized and dried thoroughly. A razor blade was used to create a wound, as described above. Upon caudal fin amputation, zebrafish were immediately placed (wound-side down) into the holding tube of the blood-collection apparatus. The collection apparatus containing a wounded fish was placed into a microcentrifuge and spun at 40 g and 15 °C for 30 s to collect blood. This method was adapted from Babaei et al. and modified to accommodate the time-sensitive nature of metabolic experiments (Babaei et al., 2013).

Immediately following all blood collections, blood was allowed to clot on ice for 10 min and then centrifugated at 1,600 g and 4 °C for 10 min to separate serum from blood cells. Serum was transferred to a new 0.5 mL microcentrifuge tube, snap frozen in liquid nitrogen, and stored at -80 °C.

METHOD DETAILS

Isotope tracing

For all isotope-tracing experiments, zebrafish were fasted for 24 h to empty the digestive tract prior to labeling. To determine the [U-^{13}C] glucose concentration for steady-state labeling, concentrations between 5 - 20 mM were tested. We determined that 10 mM [U-^{13}C] glucose was optimal, as it resulted in ~10% serum enrichment at isotopic steady state without perturbing circulating glucose levels. Similarly, concentrations between 1 - 10 mM of [U-^{13}C] glutamine were tested for steady-state labeling. For glutamine labeling experiments, 5 mM [U-^{13}C] glutamine was deemed optimal, as it yielded ~10-15% enrichment in serum glutamine without significantly altering circulating levels of glutamine. For ^{15}N-BCAA labeling experiments, 2 mM each [^{15}N] leucine, [^{15}N] isoleucine, and [^{15}N] valine were concurrently supplemented to facility water. For ^{13}C-BCAA labeling experiments, 4 mM each of [U-^{13}C] leucine, [U-^{13}C] isoleucine, and [U-^{13}C] valine were concurrently supplemented to facility water. During steady-state labeling experiments, zebrafish were allowed to swim freely in facility water containing the corresponding stable isotopes at the aforementioned concentrations, in addition to 2% penicillin/streptomycin. For isotope tracing via intraperitoneal injection, zebrafish were injected as previously described (Kinkel et al., 2010). Briefly, anesthetized fish were quickly dried and weighed. Zebrafish were then placed into the trough of a wet precut sponge, with the abdomen facing up and gills secured in the trough. A 35G beveled needle and NanoFil 10 μL syringe was carefully inserted midline near the pelvic girdle, and a [U-^{13}C] glucose treatment solution (0.5 mg/g) was slowly dispensed. After injection, fish were placed in 28 °C facility water and monitored for recovery from anesthesia (typically 5-10 seconds). Throughout the experiment, each fish was kept in an individual tank to allow for tracking.

All glassware that was used to carry out labeling experiments was washed thoroughly and autoclaved prior to experimentation. For the duration of the 24 h of labeling, fish were kept in an indoor environment at a temperature of 28 ± 1 °C with the same 14:10-h light:dark circadian cycle as described above. After 24 h of labeling, fish were anesthetized by gradual cooling, and tissues were harvested in pre-weighed 1.5 mL microcentrifuge tubes, snap frozen in liquid nitrogen, and stored at -80 °C.

Metabolite extraction

To extract metabolites from serum, samples were diluted 1:15 with methanol:acetonitrile:water (2:2:1) at -20 °C, vortexed for 10 s, and incubated at -20 °C for 1 h. Following incubation, metabolite extracts were centrifuged at 20,000 g and 4 °C for 10 min, and the supernatant was transferred into an LC-MS vial for same-day analysis. To extract metabolites from zebrafish tissues, frozen samples were ground in 1.5 mL microcentrifuge tubes with a disposable pellet pestle. The pellet pestle was placed in liquid nitrogen prior to sample grinding, and the microcentrifuge tube (containing tissue) was submerged in liquid nitrogen for the entirety of tissue grinding. We note that microcentrifuge tubes were labeled and weighed prior to tissue harvest and then weighed again following tissue grinding. The powderized tissue was mixed with -20 °C methanol:acetonitrile:water (2:2:1), and subjected to two cycles of freezing in liquid nitrogen (1 min), thawing in 25 °C water (10 s), sonication (5 min), and vortexing (30 s). Samples were then incubated at −20 °C for 1 h. For every 1 mg of tissue wet weight, 40 μL of extraction solvent was added. Following protein precipitation, tissue extracts were centrifuged at 20,000 g and 4 °C for 10 min, and the supernatant was transferred into an LC-MS vial for same-day analysis.

LC-MS analysis

Ultra-high performance LC (UHPLC)/MS was performed with a Thermo Scientific Vanquish Horizon UHPLC system interfaced with a Thermo Scientific Orbitrap ID-X Tribrid Mass Spectrometer (Waltham, MA). Hydrophilic interaction liquid chromatography (HILIC) was conducted with a SeQuant ZIC-pHILIC guard column (20 mm x 2.1 mm, 5 μm) connected to a SeQuant ZIC-pHILIC column (100 mm x 2.1 mm, 5 μm). Chromatographic solvents were adapted from previously described work (Hsiao et al., 2018; Spalding et al., 2018). Briefly, mobile phase solvents were composed of A = 20 mM ammonium acetate and 0.1% ammonium hydroxide in water:acetonitrile (95:5) and B = acetonitrile:water (95:5). Either 5 μM ammonium phosphate or 4 μM medronic acid was included in the A solvent. We applied the following linear gradient at a flow rate of 0.25 mL/min: 0 – 1 min, 90% B; 1 – 17.5 min, 45% B; 17.5 – 19 min, 30% B; 19 – 19.5 min, 30% B; 19.5 – 22 min, 90% B. The column was equilibrated with 20 column volumes of 90% B following each injection. The column compartment was maintained at 40 °C and injection volumes were 4 μL for all experiments. Data were collected with the following MS source settings: spray voltage, -3 kV; sheath gas, 35; auxiliary gas, 10; sweep gas, 1; ion transfer tube temperature, 275 °C; vaporizer temperature, 300 °C; mass range, 67 – 1000 Da; resolution, 120,000 (MS1), 60,000 (MS/MS); maximum injection time, 100 ms; isolation window, 1.5 Da. With this method, it was possible to resolve ^{15}N and ^{13}C peaks.

Please cite this article in press as: Naser et al., Isotope tracing in adult zebrafish reveals alanine cycling between melanoma and liver, Cell Metabolism (2021), https://doi.org/10.1016/j.cmet.2021.04.014

Metabolites were identified on the basis of accurate mass, MS/MS data, and retention time. All MS/MS data and retention times from compounds in research samples were matched to MS/MS data and retention times of purchased standards.

Analysis of liver weight

WT and melanoma-bearing zebrafish were euthanized and weighed, and then livers were harvested in pre-weighed microcentrifuge tubes, as described above. Liver masses were determined by subtracting the combined tissue-microcentrifuge tube mass from the pre-weighed microcentrifuge tube mass. A ratio of liver to whole-body masses of WT and melanoma-bearing zebrafish were then compared. To account for the contribution of tumors to whole-body mass, the ratio of liver to whole-body mass after subtracting the mass of tumors was also calculated. Tumor masses were determined by using an analytical balance, after isolated tumors were transferred to pre-weighed microcentrifuge tubes.

Ammonia excretion assay

Groups of WT and tumor-bearing fish were individually housed in separate tanks of fresh facility water for 24 h, without circulation. Water samples were collected at baseline and after 24 h and frozen at -80 °C until analysis. The concentration of ammonia in water was determined by using a modified Berthelot assay as described previously (Spinelli et al., 2017). Briefly, 20 μL of sampled water was mixed with 400 μL of 100 mM phenol, 50 mg/L sodium nitroprusside, 125 mM sodium hydroxide, 0.38 M sodium phosphate dibasic, and 1% sodium hypochlorite. Following mixing, samples were incubated at 37 °C for 40 min, and then absorbance was read at 670 nm. An ammonium chloride standard curve was used to quantify ammonia.

Glycogen assay

WT and melanoma-bearing zebrafish were fasted for 24 h and then euthanized, as described above, to harvest livers. Tissues were homogenized by using a disposable pellet pestle, suspended in 200 μL water, and boiled for 10 min to deactivate enzymes before analysis. Glycogen was quantified by using a commercial kit following the manufacturer's protocol. Liver protein content was determined by using a Bradford Assay with Bradford Reagent, according to the manufacturer's guidelines and a BSA standard curve.

Vemurafenib treatment

For ^{13}C-labeling experiments following drug treatment, adult zebrafish were administered 100 mg/kg vemurafenib or DMSO once per day for four or ten days. Drug dosage was selected based on previous work, which showed efficacy and no toxicity in zebrafish (Dang et al., 2016b). Vemurafenib was dissolved in DMSO for the treatment arm, and vemurafenib solution or DMSO (vehicle) was delivered via intraperitoneal injection following a previously described protocol detailed above (Kinkel et al., 2010). Throughout the experiment, each fish was kept in an individual tank to allow for tracking. After the final treatment, fish were fasted for 24 h and then exposed to 10 mM [U-^{13}C] glucose for 24 h. Serum and tissue were harvested, immediately snap frozen in liquid nitrogen, and stored at -80 °C until LC-MS analysis. For ammonia-quantification experiments, vehicle or vemurafenib solution was delivered to tumor-bearing zebrafish, as described above, for 10 days prior to water sampling.

EIPA treatment

For ^{13}C-labeling experiments following drug treatment, adult zebrafish were administered 50 μM 5-(N-ethyl-N-isopropyl)amiloride (EIPA) or DMSO. Drug dosage was adapted from previous work to mitigate toxicity in tumor-bearing animals, and administered in the same manner (Dymowska et al., 2015). Briefly, EIPA was dissolved in DMSO and 0.1% drug solution or DMSO (vehicle) were added to separate tanks of facility water. Tumor-bearing fish were randomly placed in either EIPA or vehicle conditions for a total of six days, with water changes every other day. Fish were fasted for 24 h beginning on the fourth day of treatment, and then exposed to 10 mM [U-^{13}C] glucose for 24 h. Serum and tissues were harvested, immediately snap frozen in liquid nitrogen, and stored at -80 °C until LC-MS analysis.

2-deoxyglucose and 2-aminoisobutyric acid assay

Tumor-bearing fish were placed in facility water containing 0.5 mM 2-aminoisobutyric acid (2-AIB) or 1 mM 2-deoxyglucose (2-DG) for 8 h. Fish were anesthetized, and tissues were harvested and frozen as described above. Metabolites were extracted by using the above protocol and analyzed by LC-MS. Chemical standards of 2-aminoisobutyric acid and 2-deoxyglucose 6-phosphate were used to confirm metabolite identities.

ß-chloroalanine treatment

To determine the maximum nonlethal dose of ß-chloroalanine, BRAF/p53 fish were housed in ß-chloroalanine mixed with facility water at concentrations ranging from 0.05 – 2.0 mM. Animals were housed in ß-chloroalanine-treated water for up to 5 days, with water changes every other day. Tanks were monitored frequently for animals that were experiencing acute toxicity or animals that had succumb to drug exposure, which were removed. A normal feeding schedule was maintained for all fish throughout the duration of drug treatment.

For ^{13}C-BCAA labeling experiments following drug treatment, adult zebrafish were administered 600 μM ß-chloroalanine or vehicle. ß-chloroalanine was dissolved directly in facility water, and tumor-bearing fish were randomly placed in either ß-chloroalanine or no-drug (vehicle) conditions for a total of 10 days, with water changes every other day. Fish were fasted for 24 h beginning on

the ninth day of treatment, and then exposed to 4 mM each of [U-^{13}C] leucine, [U-^{13}C] isoleucine, and [U-^{13}C] valine for 24 h. Serum and tissues were harvested, immediately snap frozen in liquid nitrogen, and stored at -80 °C until LC-MS analysis.

Histology

Adult zebrafish were euthanized via gradual cooling, and livers were rapidly dissected and placed on tin foil on dry ice. Fresh-frozen livers were embedded in carboxymethylcellulose in water (5%), solidified at -80 °C for 1 h, and then stored at -20 °C overnight. Embedded tissues were sectioned at 5 μM thickness, mounted onto glass slides, and dehydrated until staining. Glycogen staining was performed by using a periodic acid-Schiff (PAS) Kit with and without diastase according to the manufacturer's instructions. Samples were viewed on a Zeiss AxioObserver D1 inverted microscope (Carl Zeiss, Thrownwood, NY) equipped with an Axiocam 503 color camera. Appropriate areas of the tissue were identified, and images were acquired with Plan-Apochromat (NA 1.4) oil objective by using the ZEN 2 (blue edition) software.

Real-time PCR analysis

RNA was extracted from zebrafish liver samples by using Trizol. cDNA was synthesized with the SuperScript III First-Strand Synthesis SuperMix following the manufacturer's guidelines. Reverse transcripts were produced by using SuperScript II, and real-time reverse-transcription polymerase chain reaction was performed by using the PowerUp SYBR Green Master Mix with a StepOnePlus Real-Time PCR system (Applied Biosystems) according to the manufacturer's guidelines. Both elongation factor 1 alpha (EF1α) and β-actin were used as reference genes, and all primer sequences are listed in the key resources table (Li et al., 2017). All samples were run in triplicate and results were analyzed by using the $2^{-\Delta\Delta Ct}$ method.

Analysis of BCAT1 expression in zebrafish

Differential expression of the *BCAT1* gene was compared between melanoma cells and melanocytes by using RNA-seq. RNA was isolated from melanoma tumors from BRAF/p53 zebrafish and sorted melanocytes from WT zebrafish by using the Macherey Nagel Nucleospin XS kit. The Genome Technology Access Center (GTAC) prepared the samples with a Clontech SMARTer cDNA amplification kit and ran sequencing by using an Illumina HiSeq 3000 system with 1x50bp read length. GTAC performed preliminary computational data analysis by aligning reads to zv9.

Analysis of BCAT1 expression in human patients

Resected surgical melanoma tumor samples were collected in RPMI 1640 media and placed on ice. Tissue was dissociated into multiple pieces, and three to four ~1 cm pieces were flash frozen in tinfoil with liquid nitrogen. At a later date, specimens were removed from the freezer for processing. Total RNA was extracted by using RNAeasy Mini kits following the manufacturer's protocol. RNA samples were treated with RNase-free DNase and stored at -80 °C. A Tru-Seq RNA library was constructed and NovaSeq S4 was used for sequencing, with a target of 50 million read pairs per library.

Samples were quantified by using Kallisto v0.43.1 with human genome reference GRCh38 (GRCh38-2.1.0) (Bray et al., 2016). For gene-level expression estimates, we took the sum of the TPM values for transcripts of the same gene. Human melanocytes RNA-seq data were obtained from previous studies (Haltaufderhyde and Oancea, 2014; Reemann et al., 2014). For comparison, FPKM was converted to TPM by TPM = (FPKM / sum of FPKM over all genes) * 10^6. RPKM was also converted to TPM with the same formula.

QUANTIFICATION AND STATISTICAL ANALYSIS

Data analysis

LC-MS data were processed and analyzed with the open-source Skyline program as well as the Compound Discoverer 3.0 software. Natural-abundance correction of ^{13}C for tracer experiments was performed with AccuCor (Su et al., 2017). The number of biological replicates in each experiment is listed in the figure legends. Statistical analyses of LC-MS data are described in the figure legends. Unless otherwise noted, statistically significant differences were assessed by a two-tailed paired t test. Graphing was done in Microsoft Excel and GraphPad Prism.